Trajectory Tracking Control of Rowing Pectoral Fin-Actuated Robotic Fish

Maria L. Castaño, *Member, IEEE*, and Xiaobo Tan, *Fellow, IEEE*

***Abstract*—Robotic fish has received increasing attention in the last few decades, as they hold strong promise in a myriad of applications. Efficient and precise control of these robots, particularly accurate trajectory control, has become essential in many of these applications. This article proposes a dual-loop backstepping-based trajectory tracking control approach for a robotic fish actuated by rowing pectoral fins. While rowing pectoral fin-based locomotion is important for maneuvering, the range constraints of fin movement pose significant challenges in the control of robotic fish, including potentially preventing the robot from generating the thrust needed to maneuver in a desired direction. To overcome these challenges, we propose a dual-loop controller, designed based on an averaged dynamic model of the robot. In particular, an outer-loop backstepping-based controller finds the needed force and moment inputs for the robot to track the desired trajectory, while the inner loop determines the optimal fin-beat parameters such that the resulting fin-generated forces and moment are close to their desired values. Experimental results are presented to show the efficacy of the proposed control scheme, where the robot is commanded to track a trajectory with variable linear and angular velocities. Comparing to a well-tuned proportional–integral–derivative controller, the proposed control scheme shows a distinct advantage in tracking desired orientations in addition to tracking desired positions.**

***Index Terms*—Averaged model, backstepping control, robotic fish, trajectory tracking.**

I. Introduction

THE efficiency, agility, and remarkable feats in swimming of fish have inspired significant interest in developing robotic fish, with potential applications in search and rescue, environmental monitoring, and robot–animal interactions [1]–[3]. Various bio-inspired propulsion methods, from pectoral or oscillating caudal fins to undulation of the entire body [4], have been explored in the design of these robots. Although caudal fins are typically used for efficient propulsion at relatively high speeds, pectoral fins are vital for maneuvering and assisting propulsion at lower swimming speeds [5].

Pectoral fin motions are generally classified into three modes based on the axis of rotation: rowing, feathering, and flapping. Feathering and flapping involve fin rotation about the transverse and longitudinal axis, respectively, while rowing involves fin rotation about the vertical axis. Rowing motion is classified as a "drag-based" swimming mechanism, where the drag element of fluid dynamics generates the thrust. Furthermore, it can be effective in realizing a number of maneuvering tasks, such as sideway swimming, forward swimming, and turning [6]. In the rowing motion, the fin beat cycle comprises two submovements: a power stroke, during which the pectoral fin rotates toward the back of the robot and produces thrust through the induced drag on the fin surface, and a recovery stroke, where the fin moves toward the front of the body, ideally with minimal loading, to get ready for the next fin-beat cycle.

Accurate trajectory tracking is essential to many applications of robotic fish, for instance, when sampling specific areas or seeking pollutant sources. There has been limited work reported on the control of pectoral fin-actuated robotic fish. For example, some work has focused on open-loop motion control, where the generation of fish-like swimming gaits is considered [7]–[10]. Several authors have proposed closed-loop control methods based on sensory-feedback central pattern generators (CPGs) to achieve target tracking or obstacle avoidance [11]–[13]. Kato [14] proposed fuzzy rules-based control laws to drive a robotic fish to rendezvous and dock in a three-dimensional workspace. In [15] geometric control methods were used to achieve closed-loop depth control of a robotic fish using pectoral fins undergoing feathering motion. The aforementioned work has been largely based on motion primitives (which can be system-specific) or focused on heading, depth, and velocity tracking for robotic fish using pectoral fins undergoing feathering or lead-lag motion.

Although beneficial for in-plane locomotion, utilizing rowing motion for propulsion and maneuvering presents challenges in control robotic fish. These challenges lie with the fin movement constraints and the mechanism of how the "drag-based" swimming method generates thrust. Once the fin reaches its maximum angular position, it has to first row in the opposite direction (which generates undesirable drag), in order to make room to be able to generate the desired thrust. For example, to propel the

Manuscript received January 21, 2022; revised March 27, 2022; accepted April 29, 2022. Recommended by Technical Editor M. Grebenstein and Senior Editor X. Chen. This work was supported in part by the National Science Foundation under Grant DGE1424871, Grant ECCS 1446793, Grant IIS 1715714, and Grant IIS 1848945. *(Corresponding author: Maria L. Castaño.)*

Maria L. Castaño is with the Johns Hopkins University Applied Physics Lab, Laurel, MD 20723 USA (e-mail: castanom@msu.edu).

Xiaobo Tan is with the Department of Electrical and Computer Engineering, Michigan State University, East Lansing, MI 48824 USA (e-mail: xbtan@msu.edu).

Color versions of one or more figures in this article are available at https://doi.org/10.1109/TMECH.2022.3175765.

Digital Object Identifier 10.1109/TMECH.2022.3175765

robot, a forward thrust is needed, which can only be generated during the power stroke of the pectoral fin; once the fin has reached its maximum angular position, it has to recover in order to be able to generate forward thrust again. During the recovery phase, however, the fin will produce a unwanted thrust that would thrust the robot backwards. Coordinating optimal fin movement while handling these actuation constraints with rigorous control design is challenging. To the best of our knowledge, systematic trajectory tracking control approaches that accommodate the input constraints and have closed-loop stability guarantees have not been proposed for robotic fish with pectoral fins undergoing rowing motion.

In this article, we propose a dual-loop backstepping-based controller for trajectory tracking of a robotic fish actuated by a pair of rigid pectoral fins undergoing rowing motion. By considering the general nature of cyclic actuation, the control design is based on an averaged dynamic model, where the hydrodynamic force generated by the pectoral fins is captured using the blade element theory [16]. In this design, the physical control inputs involve two of the fin-beat parameters, the bias, and the power to recovery stroke ratio, while the other parameters (fin-beat period and bias) are kept constant. Dual-loop control paradigms, which separates the controller implementation into two hierarchical levels and thus facilitates the synthesis, have been used in multiple contexts, such as motion control of manipulators [17], mode transition control for hybrid electric vehicles [18], and robust control of wind turbines [19]. In our work, a dual-loop design paradigm allows us to treat the robotic fish with pectoral fins as a cascaded system, facilitating the control synthesis and handling of actuation constraints. In particular, we consider the robotic fish and the fins as separate, interconnected systems. Backstepping-based control design presents a systematic, computationally inexpensive method for trajectory tracking control and allows the handling of input constraints while guaranteeing stability [20]. The proposed scheme thus uses a backstepping-based outer-loop controller to find the needed hydrodynamic forces and moment inputs for the robot to track the desired trajectory. The inner loop then uses a multivariable minimization solver to determine the optimal fin-beat parameters such that the achieved forces and moment are close to their desired values.

To demonstrate the effectiveness of the proposed scheme, we present experimental results on tracking a trajectory with variable linear and angular velocities. Furthermore, we compare the proposed control with a well-tuned proportional–integral–derivative controller. In particular, we compare the mean position and heading tracking error performance for both controllers across five trials. The averaged position and orientation error scores results show the proposed backstepping-based approach has better performance than PID in terms of tracking the position, but it significantly outperforms the PID controller in terms of tracking the desired orientations.

Our recent work [21] proposed a similar dual-loop approach to achieve maneuvering control based on the original dynamic model (instead of an averaged dynamic model); however, it was limited to tracking only body-fixed surge and angular velocities (instead of reference position/orientation trajectories) and was evaluated only with simulation. In addition, the inner-loop model-predictive fin motion planning algorithm in [21] was computational-intensive, making it difficult if not infeasible to implement in real time. Some of our previous works focused on (single-loop) trajectory tracking and path following control for robotic fish actuated by a tail fin [20], [22], where backstepping control and model predictive control were used, respectively. Compared with the case of tail-actuation, control of robotic fish actuated by pectoral fins is significantly more difficult. Developing an effective real-time control strategy for the latter case, as proven in experiments, is the central contribution of this current article.

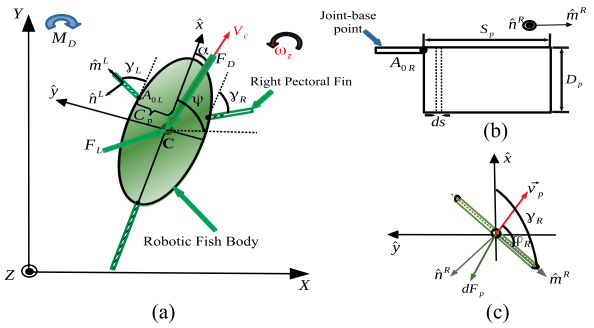

Fig. 1. (a) Top view of a robotic fish actuated by pectoral fins undergoing planar motion. (b) Side view of the right pectoral fin with its parameters. (c) top view of the pectoral fin with its associated forces and angles. [21].

The rest of this article is organized as follows. We first briefly review the dynamic and averaged models for a rowing pectoral fin-actuated robotic fish in Section II. In Section III, the problem of trajectory tracking is formulated, followed by the presentation of the backstepping control design. In Section IV experimental results on trajectory tracking are presented and discussed. Finally, Section V concludes this article.

II. Models for Pectoral Fin-Actuated Robotic Fish

In this section, we first review the dynamic model for a robotic fish actuated by rowing pectoral fins, and then present the corresponding averaged dynamic model, which is used for the model-based control design.

A. Original Dynamic Model

As done in [21], the pectoral fin-actuated robotic fish is modeled as a rigid body with rigid pectoral fins that are actuated at their corresponding bases, and it is assumed that the robot operates in an irrotational, inviscid, and incompressible fluid within an infinite domain [23].

As illustrated in Fig. 1(a), we define $[X,Y,Z]^T$ as the inertial coordinate system and $[\hat{x},\hat{y},\hat{z}]^T$ as the body-fixed coordinate system. The velocity vector of the center of mass in the body-fixed coordinates is given as $\boldsymbol{V}_c = [v_{c_x}, v_{c_y}, v_{c_z}]$, where v_{c_x}, v_{c_y}, and v_{c_z} correspond to the surge, sway, and heave velocities, respectively. On the other hand, $\omega = [\omega_x, \omega_y, \omega_z]$, denotes the angular velocity expressed in the body-fixed coordinate, where ω_x, ω_y, ω_z correspond to the roll, pitch, and yaw motions,

respectively. Let C_p be the distance between the body's center of mass and the pectoral fin base, and A_{0R} and A_{0L} denote the pivot points for the right and left fins, respectively. Furthermore, γ_L and γ_R denote the angles formed by the left and the right pectoral fin, respectively, with the body-fixed $\hat{x}$-axis. Finally, we consider the pectoral fins to be rigid and rectangular with chord length D_p and span length S_p.

In this work, only the planar motion is considered, and it is assume that the body is symmetric with respect to the $\hat{x}\hat{z}$-plane and that the pectoral fins move in the $\hat{x}\hat{y}$-plane. As a result, the system only has three degrees of freedom, namely, surge (v_{c_x}), sway (v_{c_y}), and yaw (ω_z). It is further assumed that the inertial coupling between yaw, sway, and surge motions can be neglected [24], which leads to the following simplified equations of planar motion:

$$(m_b - m_{a_x})\dot{v}_{c_x} = (m_b - m_{a_y})v_{c_y}\omega_z + f_x \tag{1}$$

$$(m_b - m_{a_y})\dot{v}_{c_y} = -(m_b - m_{a_x})v_{c_x}\omega_z + f_y \tag{2}$$

$$(J_{bz} - J_{a_z})\dot{\omega}_z = (m_{a_y} - m_{a_x})v_{c_x}v_{c_y} + \tau_z \tag{3}$$

where J_{bz} is the inertia of the body about the $\hat{z}$-axis, m_b is the mass of the body, m_{a_x} and m_{a_y} are the hydrodynamic derivatives that represent the added masses of the robotic fish along the $\hat{x}$ and $\hat{y}$ directions, respectively, and J_{a_z} represents the added inertia effect of the body about the $\hat{z}$ direction. Furthermore, we let α denote the angle of attack, given by $\alpha = \arctan(\frac{v_{c_y}}{v_{c_x}})$, and let the heading angle, formed by the $\hat{x}$-axis relative to the X-axis, be denoted by ψ. Finally, f_x, f_y, and τ_z are the hydrodynamic forces and moment due to the pectoral fin actuation and the body-fluid interactions and are given by

$$f_x = f_{h_x} - F_D\cos(\alpha) + F_L\sin(\alpha) \tag{4}$$

$$f_y = f_{h_y} - F_D\sin(\alpha) - F_L\sin(\alpha) \tag{5}$$

$$\tau_z = \tau_{h_z} + M_D \tag{6}$$

where F_D, F_L, and M_D are the body drag, lift, and moment, respectively, and f_{h_x}, f_{h_y}, and τ_{h_z} are the hydrodynamic forces and moment transmitted to the fish body by the right and left pectoral fins.

The final dynamic model augmented with the kinematic equations can be summarized as follows:

$$\begin{bmatrix} \dot{X} \\ \dot{Y} \\ \dot{\psi} \\ \dot{v}_{c_x} \\ \dot{v}_{c_y} \\ \dot{\omega}_z \end{bmatrix} = \begin{bmatrix} v_{c_x}\cos\psi - v_{c_y}\sin\psi \\ v_{c_x}\sin\psi + v_{c_y}\cos\psi \\ \omega_z \\ f_1(v_{c_x}, v_{c_y}, \omega_z) + \dfrac{f_{h_xR} + f_{h_xL}}{m_1} \\ f_2(v_{c_x}, v_{c_y}, \omega_z) + \dfrac{f_{h_yR} + f_{h_yL}}{m_2} \\ f_3(v_{c_x}, v_{c_y}, \omega_z) + \dfrac{\tau_{h_R} + \tau_{h_L}}{J_3} \end{bmatrix} \tag{7}$$

where

$$\begin{cases} f_1(v_{c_x}, v_{c_y}, \omega_z) = \dfrac{m_2}{m_1}v_{c_y}\omega_z - \dfrac{c_1}{m_1}v_{c_x}\sqrt{v_{c_x}^2 + v_{c_y}^2} + \\ \qquad\qquad \dfrac{c_2}{m_1}v_{c_y}\sqrt{v_{c_x}^2 + V_{c_y}^2}\ \arctan\left(\dfrac{v_{c_y}}{v_{c_x}}\right) \\ f_2(v_{c_x}, v_{c_y}, \omega_z) = -\dfrac{m_1}{m_2}v_{c_x}\omega_z - \dfrac{c_1}{m_2}v_{c_y}\sqrt{v_{c_x}^2 + v_{c_y}^2} \\ \qquad\qquad -\dfrac{c_2}{m_2}v_{c_x}\sqrt{v_{c_x}^2 + v_{c_y}^2}\ \arctan\left(\dfrac{v_{c_y}}{v_{c_x}}\right) \\ f_3(v_{c_x}, v_{c_y}, \omega_z) = \dfrac{(m_1 - m_2)}{J_3}v_{c_x}v_{c_y} - c_4\omega_z^2\mathrm{sgn}(\omega_z) \end{cases} \tag{8}$$

with $m_1 = m_b - m_{a_x}, m_2 = m_b - m_{a_y}, J_3 = J_{bz} - J_{a_z}, c_1 = \frac{1}{2}\rho S C_D,\ c_2 = \frac{1}{2}\rho S C_L,\ c_4 = \frac{1}{(J_3)}C_M$. ρ is the density of water, S_A is the wetted surface area for the robot, C_D, C_L, and C_M are the drag force coefficient, lift force coefficient, and the drag moment coefficient, respectively. sgn$(\cdot)$ is the signum function. Finally, the subscripts R and L correspond to the right and left pectoral fin, respectively. We use f_{h_x}, f_{h_y}, and τ_h along with the subscripts R and L to denote the the hydrodynamic forces and moment transmitted to the fish body by the right and left pectoral fin, respectively. We refer the reader to [21], [25] for a more detailed derivation of the hydrodynamic forces.

B. Averaged Dynamic Model

The rowing pectoral fins sweep back and forth within the frontal plane. In order to generate a net thrust, the pectoral fins need distinct power and recovery strokes actuation. For example, to generate net forward thrust the fin has to be actuated faster in the power stroke than in the recovery stroke. We let fin beat pattern be defined as follows:

$$\gamma(t) = \begin{cases} \gamma_0 - \gamma_A\cos\left[\pi\dfrac{(\zeta+1)}{T_p}t\right], & 0 \le t \le \dfrac{T_p}{\zeta+1} \\ \gamma_0 + \gamma_A\cos\left[\pi\left(\dfrac{\zeta+1}{\zeta T_p}\right)(t - \dfrac{T_p}{\zeta+1})\right], & \\ \qquad \dfrac{T_p}{\zeta+1} < t \le T_p \end{cases} \tag{9}$$

where γ_A is the fin-beat amplitude, γ_0 is the fin-beat bias, T_P is the fin-beat period, and ζ is the ratio of the angular velocities of the fin during the power and recovery strokes, respectively.

Considering this periodic fin movement, one can develop an averaged dynamic model for the robotic fish, through proper scaling of the fin-generated hydrodynamic forcing terms and then classical averaging, as proposed in [16]. Let the subscripts R and L correspond to the right and left pectoral fin, respectively, such that the scaled-averaged dynamics can be summarized as

follows:

$$\begin{cases} \dot{\bar{v}}_{c_x} = & f_1(\bar{v}_{c_x}, \bar{v}_{c_y}, \bar{\omega}_z) + K_{f_xR} \cdot \bar{f}_{h_xR}(\gamma_{0R}, \gamma_{AR}, T_{pR}, \zeta_R) \\ & + K_{f_xL} \cdot \bar{f}_{h_xL}(\gamma_{0L}, \gamma_{AL}, T_{pL}, \zeta_L) \\ \dot{\bar{v}}_{c_y} = & f_2(\bar{v}_{c_x}, \bar{v}_{c_y}, \bar{\omega}_z) + K_{f_yR} \cdot \bar{f}_{h_yR}(\gamma_{0R}, \gamma_{AR}, T_{pR}, \zeta_R) \\ & + K_{f_yL} \cdot \bar{f}_{h_yL}(\gamma_{0L}, \gamma_{AL}, T_{pL}, \zeta_L) \\ \dot{\bar{\omega}}_z = & f_3(\bar{v}_{c_x}, \bar{v}_{c_y}, \bar{\omega}_z) + K_{m_R} \cdot \bar{\tau}_{h_R}(\gamma_{0R}, \gamma_{AR}, T_{pR}, \zeta_R) \\ & + K_{m_L} \cdot \bar{\tau}_{h_L}(\gamma_{0L}, \gamma_{AL}, T_{pL}, \zeta_L) \end{cases} \tag{10}$$

where the right pectoral fin hydrodynamic forces and moment are given by

$$\bar{f}_{h_xR} = \frac{D_p \lambda S_p^3 \pi^2 \rho \gamma_{0R} \gamma_{AR}^2 (-4\gamma_{0R}^2 - 3(-8+\gamma_{AR}^2))(-1+\zeta_R^2)}{288 m_1 \zeta_R T_{pR}^2} \tag{11}$$

$$\begin{aligned} \bar{f}_{h_yR} = \frac{-\gamma_A^2 S_p \pi^2}{96 m_2 T_{pR}^2 \zeta} & \left(4 D_p \gamma_{0R}^2 \lambda S_p^2 \rho(-1+\zeta_R^2)\right. \\ & + D_p(-8+\gamma_{AR}^2)\lambda S_p^2 \rho(-1+\zeta_R^2) - 4\gamma_{0R}^3 m_p (1+\zeta_R)^2 \\ & \left. - 3\gamma_{0R}\gamma_{AR}^2 m_p (1+\zeta_R)^2\right) \end{aligned} \tag{12}$$

$$\begin{aligned} & \bar{\tau}_{h_R} \\ & = \frac{C_p D_p \lambda S_p^3 \pi^2 \rho \gamma_{0R} \gamma_{AR}^2 (-4\gamma_{0R}^2 - 3(-8+\gamma_{AR}^2))(-1+\zeta_R^2)}{288 J_3 \zeta_R T_{pR}^2} \end{aligned} \tag{13}$$

λ is the fin's normal force coefficient, and K_{f_x}, K_{f_y}, K_m along with the subscripts R and L are the force and moment scaling functions for the right and left pectoral fins, respectively, and are dependent on its corresponding fin-beat parameters. We refer the reader to [16] for a more comprehensive derivation of the averaged model and the methods for identifying its scaling functions and parameters.

III. Model-Based Trajectory Tracking Control

A. Trajectory Tracking Problem

Let the vectors $\bar{\mathbf{F}}(t) = [X\ Y\ \psi]^T$ and $\bar{\mathbf{T}}(t) = [X_r\ Y_r\ \psi_r]^T$ denote the position (of the center) and orientation of the robotic fish and the desired position/orientation of a reference robot, respectively, with respect to the inertial frame {I} at a given time t. Furthermore, we let u_r, v_r, ω_r be the body-fixed velocities of the reference robot, where its longitudinal axis is defined by ψ_r. Let $\boldsymbol{e}_\chi = [X_e\ Y_e\ \psi_e]^T$ denote the tracking error vector expressed in the robot's body-fixed frame

$$\boldsymbol{e}_\chi = {}^I\boldsymbol{R}_B(\bar{\mathbf{F}} - \bar{\mathbf{T}}) \tag{14}$$

where ${}^I\boldsymbol{R}_B$ is the rotation matrix from the inertial frame {I} to the body-fixed frame {B}

$${}^I\boldsymbol{R}_B = \begin{bmatrix} \cos\psi & \sin\psi & 0 \\ -\sin\psi & \cos\psi & 0 \\ 0 & 0 & 1 \end{bmatrix}. \tag{15}$$

The derivative of $\boldsymbol{e}_\chi$ (expressed in {B}) is given by

$$\begin{aligned} \frac{\mathrm{d}\boldsymbol{e}_\chi}{\mathrm{d}t} = & \bar{\boldsymbol{S}} \begin{pmatrix} {}^I\boldsymbol{R}_B & 0_{2\times 1} \\ 0_{1\times 2} & 1 \end{pmatrix} (\bar{\mathbf{F}} - \bar{\mathbf{T}}) \\ & + \begin{pmatrix} {}^I\boldsymbol{R}_B & 0_{2\times 1} \\ 0_{1\times 2} & 1 \end{pmatrix} \left(\frac{\mathrm{d}\bar{\mathbf{F}}}{\mathrm{d}t} - \frac{\mathrm{d}\bar{\mathbf{T}}}{\mathrm{d}t} \right) \end{aligned} \tag{16}$$

where

$$\bar{\boldsymbol{S}} = \begin{bmatrix} 0 & \omega & 0 \\ -\omega & 0 & 0 \\ 0 & 0 & 0 \end{bmatrix}. \tag{17}$$

With (16), the following error state model, augmented with the averaged dynamics (10), is obtained

$$\begin{bmatrix} \dot{X}_e \\ \dot{Y}_e \\ \dot{\psi}_e \\ \dot{\bar{v}}_{c_x} \\ \dot{\bar{v}}_{c_y} \\ \dot{\bar{\omega}}_z \end{bmatrix} = \begin{bmatrix} \bar{v}_{c_x} - V_r \cos(\psi_e - \bar{\psi}_r) + \bar{\omega}_z Y_e \\ \bar{v}_{c_y} + V_r \sin(\psi_e - \bar{\psi}_r) - \bar{\omega}_z X_e \\ \bar{\omega}_z - \omega_r \\ f_1 + K_{f_xR} \cdot \bar{f}_{h_xR} + K_{f_xL} \cdot \bar{f}_{h_xL} \\ f_2 + K_{f_yR} \cdot \bar{f}_{h_yR} + K_{f_yL} \cdot \bar{f}_{h_yL} \\ f_3 + K_{m_R} \cdot \bar{\tau}_{h_R} + K_{m_L} \cdot \bar{\tau}_{h_L} \end{bmatrix} \tag{18}$$

where $V_r = \sqrt{\dot{u}_r^2 + \dot{v}_r^2}$, $\bar{\psi}_r = \arctan(\frac{v_r}{u_r})$, and $\omega_r = \dot{\psi}$.

By formulating the trajectory tracking problem in terms of the error dynamics, the control objective is to find a control law such that, for an arbitrary initial error, the position and orientation error states (X_e, Y_e, ψ_e) of system (18) is stabilized at the origin.

B. Trajectory Tracking Control Algorithm

To design the controller, let the control inputs be chosen as the effective fin-generated hydrodynamic forces and moment

$$u_1 = K_{f_xR} \cdot \bar{f}_{h_xR} + K_{f_xL} \cdot \bar{f}_{h_xL} \tag{19}$$

$$u_2 = K_{f_yR} \cdot \bar{f}_{h_yR} + K_{f_yL} \cdot \bar{f}_{h_yL} \tag{20}$$

$$u_3 = K_{m_R} \cdot \bar{\tau}_{h_R} + K_{m_L} \cdot \bar{\tau}_{h_L} \tag{21}$$

such that the averaged dynamic model (10) is expressed in the control-affine form as

$$\begin{bmatrix} \dot{\bar{v}}_{c_x} \\ \dot{\bar{v}}_{c_y} \\ \dot{\bar{\omega}}_z \end{bmatrix} = \begin{bmatrix} f_1(\bar{v}_{c_x}, \bar{v}_{c_y}, \bar{\omega}_z) + u_1 \\ f_2(\bar{v}_{c_x}, \bar{v}_{c_y}, \bar{\omega}_z) + u_2 \\ f_3(\bar{v}_{c_x}, \bar{v}_{c_y}, \bar{\omega}_z) + u_3 \end{bmatrix}. \tag{22}$$

To achieve trajectory tracking, we use a backstepping controller that determines the inputs u_1, u_2, and u_3 needed such that $(X_e, Y_e, \psi_e) \to 0$. We then determine the fin-beat parameters, considering their practical constraints, such that the generated force and moment inputs are close to their desired values. The states of an auxiliary system capture the mismatch between the generated and desired input values, and is used jointly with the backstepping controller to guarantee closed-loop stability, as is similarly done in [20] and [26]. Fig. 2 illustrates the control scheme. We elaborate the controller design below.

1) Outer-Loop: Backstepping Control Design: Let v_1, v_2, and v_3 represent the nominal inputs from the backstepping design, and let u_1, u_2, and u_3 be the inputs that can be practically implemented. The effect that arises due to the mismatch between the nominal and actual inputs is analyzed with the following

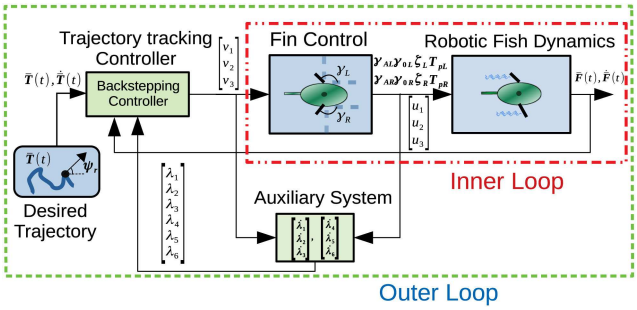

Fig. 2. Illustration of the proposed dual-loop control scheme for a robotic fish actuated with rowing pectoral fins. The green dashed line encompasses the outer loop backstepping-based trajectory tracking controller, while red dotted and dashed line encompasses the inner loop fin parameter optimization algorithm.

auxiliary system:

$$\begin{cases} \dot{\lambda}_1 = -\zeta_1\lambda_1 + \lambda_2 \\ \dot{\lambda}_2 = -\zeta_2\lambda_2 + (u_1 - v_1) + Y_e(u_3 - v_3) \\ \dot{\lambda}_3 = -\zeta_3\lambda_3 + \lambda_4 \\ \dot{\lambda}_4 = -\zeta_4\lambda_4 + (u_2 - v_2) - X_e(u_3 - v_3) \\ \dot{\lambda}_5 = -\zeta_5\lambda_5 + \lambda_6 \\ \dot{\lambda}_6 = -\zeta_6\lambda_6 + (u_3 - v_3) \end{cases} \tag{23}$$

where $\zeta_1, \zeta_2, \zeta_3, \zeta_4, \zeta_5, \zeta_6$ are positive tuning constants. The variables λ_1, λ_3, and λ_5 capture the propagated, filtered effect of the nonachievable portion of the inputs.

To stabilize the $\boldsymbol{e}_\chi$ error while also considering the mismatch between nominal and achievable inputs, we define the following Lyapunov function:

$$V_1(\bar{X}_e, \bar{Y}_e, \bar{\psi}_e) = \frac{1}{2}\bar{X}_e^2 + \frac{1}{2}\bar{Y}_e^2 + \frac{1}{2}\bar{\psi}_e^2 \tag{24}$$

where $\bar{X}_e = X_e - \lambda_1, \bar{Y}_e = Y_e - \lambda_3$ and $\bar{\psi}_e = \psi_e - \lambda_5$, are the modified tracking errors. The time derivative of (24) is given by

$$\begin{aligned} \dot{V}_1 = \bar{X}_e(&\bar{v}_{c_x} - V_r\cos(\psi_e - \bar{\psi}_r) + \bar{\omega}_z Y_e + \zeta_1\lambda_1 - \lambda_2) \\ &+ \bar{Y}_e(\bar{v}_{c_y} + V_r\sin(\psi_e - \bar{\psi}_r) - \bar{\omega}_z X_e + \zeta_3\lambda_3 - \lambda_4) \\ &+ \bar{\psi}_e(\bar{\omega}_z - \omega_r + \zeta_5\lambda_5 - \lambda_6). \end{aligned} \tag{25}$$

Let $\alpha_1 = \bar{v}_{c_x}, \alpha_2 = \bar{v}_{c_y}$ and $\alpha_3 = \bar{\omega}_z$ denote the virtual inputs with α_{d1}, α_{d2}, and α_{d3} as the corresponding desired virtual inputs. The modified virtual input errors are then defined as

$$\bar{Z}_1 = \alpha_1 - \alpha_{d1} - \lambda_2 \tag{26}$$

$$\bar{Z}_2 = \alpha_2 - \alpha_{d2} - \lambda_4 \tag{27}$$

$$\bar{Z}_3 = \alpha_3 - \alpha_{d3} - \lambda_6. \tag{28}$$

Let the desired virtual inputs be given by

$$\alpha_{d1} = V_r\cos(\psi_e - \bar{\psi}_r) - \bar{\omega}_z Y_e - \zeta_1\lambda_1 - K_{\bar{X}_e}\bar{X}_e \tag{29}$$

$$\alpha_{d2} = -V_r\sin(\psi_e - \bar{\psi}_r) + \bar{\omega}_z X_e - \zeta_3\lambda_3 - K_{\bar{Y}_e}\bar{Y}_e \tag{30}$$

$$\alpha_{d3} = \omega_r - \zeta_5\lambda_5 - K_{\bar{\psi}_e}\bar{\psi}_e \tag{31}$$

such that (25) becomes

$$\dot{V}_1 = \bar{X}_e(\bar{Z}_1 - K_{\bar{X}_e}\bar{X}_e) + \bar{Y}_e(\bar{Z}_2 - K_{\bar{Y}_e}\bar{Y}_e) + \bar{\psi}_e(\bar{Z}_3 - K_{\bar{\psi}_e}\bar{\psi}_e) \tag{32}$$

where $K_{\bar{X}_e}$, $K_{\bar{Y}_e}$, and $K_{\bar{\psi}_e}$ are positive tuning constants.

To account for the virtual input errors, we then define a new Lyapunov function

$$\bar{V}_2 = \bar{V}_1 + \frac{1}{2}\bar{Z}_1^2 + \frac{1}{2}\bar{Z}_2^2 + \frac{1}{2}\bar{Z}_3^2 \tag{33}$$

with its time derivative given by

$$\dot{\bar{V}}_2 = \dot{\bar{V}}_1 + \dot{\bar{Z}}_1\bar{Z}_1 + \dot{\bar{Z}}_2\bar{Z}_2 + \dot{\bar{Z}}_3\bar{Z}_3 \tag{34}$$

Eq. (34) can be further expanded using (10) along with the input definition (19). We choose v_1, v_2, and v_3 such that

$$\begin{aligned} \dot{\bar{V}}_2 = &-K_{\bar{X}_e}\bar{X}_e^2 - K_{\bar{Y}_e}\bar{Y}_e^2 - K_{\bar{\psi}_e}\bar{\psi}_e^2 + \bar{X}_e\bar{Z}_1 \\ &+ \bar{Y}_e\bar{Z}_2 + \bar{\psi}\bar{Z}_3 - K_1\bar{Z}_1^2 - K_2\bar{Z}_2^2 - K_3\bar{Z}_3^2. \end{aligned} \tag{35}$$

In particular, v_1, v_2, and v_3 are given by

$$\begin{bmatrix} v_1 \\ v_2 \\ v_3 \end{bmatrix} = \begin{bmatrix} 1 & 0 & Y_e \\ 0 & 1 & -X_e \\ 0 & 0 & 1 \end{bmatrix}^{-1} \begin{bmatrix} \Gamma_1 \\ \Gamma_2 \\ \Gamma_3 \end{bmatrix} \tag{36}$$

where

$$\begin{aligned} \Gamma_1 = &-f_1 - f_3 Y_e + \dot{V}_r\cos(\psi_e - \bar{\psi}_r) \\ &- V_r\sin(\psi_e - \bar{\psi}_r)(\dot{\psi}_e - \dot{\bar{\psi}}_r) - \bar{\omega}_z\dot{Y}_e \\ &- K_{\bar{X}_e}\dot{\bar{X}}_e - \zeta_1(-\zeta_1\lambda_1 + \lambda_2) - \zeta_2\lambda_2 - K_1\bar{Z}_1 \end{aligned} \tag{37a}$$

$$\begin{aligned} \Gamma_2 = &-f_2 + f_3 X_e - \dot{V}_r\sin(\psi_e - \bar{\psi}_r) + \bar{\omega}_z\dot{X}_e \\ &- V_r\cos(\psi_e - \bar{\psi}_r)(\dot{\psi}_e - \dot{\bar{\psi}}_r) \\ &- K_{\bar{Y}_e}\dot{\bar{Y}}_e - \zeta_3(-\zeta_3\lambda_3 + \lambda_4) - \zeta_4\lambda_4 - K_2\bar{Z}_2 \end{aligned} \tag{37b}$$

$$\begin{aligned} \Gamma_3 = &-f_3 + \dot{\omega}_r - \zeta_5(-\zeta_5\lambda_5 + \lambda_6) - \zeta_6\lambda_6 \\ &- K_{\bar{\psi}_e}\dot{\bar{\psi}}_e - K_3\bar{Z}_3. \end{aligned} \tag{37c}$$

By adding and subtracting $\frac{1}{4K_{\bar{X}_e}}\bar{Z}_1^2$, $\frac{1}{4K_{\bar{Y}_e}}\bar{Z}_2^2$ and $\frac{1}{4K_{\bar{\psi}_e}}\bar{Z}_3^2$ to (35), and after completing the squares one can arrive at

$$\begin{aligned} \dot{\bar{V}}_2 = &-K_{\bar{X}_e}\left(\bar{X}_e - \frac{1}{2K_{\bar{X}_e}}\bar{Z}_1\right)^2 - K_{\bar{Y}_e}\left(\bar{Y}_e - \frac{1}{2K_{\bar{Y}_e}}\bar{Z}_2\right)^2 \\ &- K_{\psi_e}\left(\bar{\psi}_e - \frac{1}{2K_{\bar{\psi}_e}}\bar{Z}_3\right)^2 - \bar{Z}_1^2\left(K_1 - \frac{1}{4K_{\bar{X}_e}}\right) \\ &- \bar{Z}_2^2\left(K_2 - \frac{1}{4K_{\bar{Y}_e}}\right) - \bar{Z}_3^2\left(K_3 - \frac{1}{4K_{\bar{\psi}_e}}\right). \end{aligned} \tag{38}$$

If $K_{\bar{X}_e} > 0, K_{\bar{Y}_e} > 0, K_{\bar{\psi}_e} > 0, K_1 > \frac{1}{4K_{\bar{X}_e}}, K_2 > \frac{1}{4K_{\bar{Y}_e}}$ and $K_3 > \frac{1}{4K_{\bar{\psi}_e}}$, then $\dot{\bar{V}}_2 < 0$ unless when $\bar{X}_e = \bar{Y}_e = \bar{\psi}_e = \bar{Z}_1 = \bar{Z}_2 = \bar{Z}_3 = 0$, which implies the convergence of $(\bar{X}_e, \bar{Y}_e, \bar{\psi}_e)$ to zero as time approaches infinity. Furthermore, since

$0 \leq \bar{V}_1(t) \leq \bar{V}_1(0)$, it can be concluded that $(\bar{X}_e, \bar{Y}_e, \bar{\psi}_e)$ belongs to $\mathcal{L}_2$. This implies that the modified tracking errors $\bar{X}_e, \bar{Y}_e$ and $\bar{\psi}_e$ do not diverge even when the desired force and moment are not achieved. Note that although the convergence for the modified tracking errors $(\bar{X}_e, \bar{Y}_e, \bar{\psi}_e)$ is guaranteed, the convergence of the actual tracking errors (X_e, Y_e, ψ_e) is not. The latter may actually increase during periods when the desired force and moment inputs cannot be implemented (i.e. $u_1 \neq v_1$, $u_2 \neq v_2$ and/or $u_3 \neq v_3$). However, when the input limitations are not in effect, and λ_1, λ_2, and λ_3 approach zero, $(\bar{X}_e, \bar{Y}_e, \bar{\psi}_e)$ converges toward (X_e, Y_e, ψ_e) and the tracking errors can be stabilized.

2) Inner Loop: Fin Parameter Optimization: Let v_1, v_2, and v_3 represent the nominal inputs obtained from the backstepping design. One needs to determine the (feasible) fin-beat parameters such that the resultant inputs u_1, u_2, and u_3 are close to v_1, v_2, and v_3, respectively. To ease the discussion, in this work, we fix $\gamma_{0R}, \gamma_{0L}, T_{pR}$, and T_{pL}, leaving $\gamma_{AR}, \gamma_{AL}, \zeta_R$, and ζ_L as the fin parameters to be found. Note that by manipulating the power to recovery ratio, one can control the robot to achieve both forward and backward swimming (for example, when $0 < \zeta_R < 1$, the right pectoral fin generates negative thrust). We use a constrained multivariable minimization solver, in particular, a controlled, elitist genetic algorithm available in MATLAB (a variant of NSGA-II [27]), to find the best fin parameters at every instant t. Furthermore, to simplify the optimization problem, we assume that the left and right power-to-recovery stroke ratios are the same such that $\zeta_R = \zeta_L = \zeta_f$. Given v_1, v_2, and v_3, the constrained multivariable optimization problem at time t is posed as

$$\underset{\gamma_{AR},\gamma_{AL},\zeta_f}{\text{argmin}} \begin{cases} Q_x(K_{f_xR} \cdot \bar{f}_{h_xR} + K_{f_xL} \cdot \bar{f}_{h_xL} - v_1)^2 \\ + \ Q_y(K_{f_yR} \cdot \bar{f}_{h_yR} + K_{f_yL} \cdot \bar{f}_{h_yL} - v_2)^2 \\ + \ Q_w(K_{m_R} \cdot \bar{\tau}_{h_R} + K_{m_L} \cdot \bar{\tau}_{h_L} - v_3)^2 \end{cases}$$

$$\text{subject to: } \gamma_{AR}, \gamma_{AL} \in [\gamma_{A\min}, \gamma_{A\max}]$$

$$\zeta_f \in [\zeta_{f\min}, \zeta_{f\max}] \tag{39}$$

where $[\gamma_{A\min}, \gamma_{A\max}]$ and $[\zeta_{f\min}, \zeta_{f\max}]$ represent the ranges of the fin-beat amplitude and power-to-recovery stroke ratio, respectively, and Q_x, Q_y, Q_w are weighting scalars.

IV. Experimental Results

A. Experimental Setup

To validate the proposed control approach, we conduct experiments using the free-swimming robotic fish shown in Fig. 3. The robot consists of a rigid-shell body, two rigid pectoral fins, and a tail, which were all 3D-printed. Note that the tail-actuation is not included in this article. To actuate the pectoral fins, Two Hitec digital microwaterproof servos (HS-5086WP) are used, while a Microchip Digital Signal Processor and Controller (DSPIC30F6014) is used to control the servos. Two Tenergy Li-Ion rechargeable batteries (7.4 V, 3350mAh) are used to power the robot, and a Xbee module is used to communicate wirelessly with a computer. The body and fin dimensions of the robot, as well as the identified parameters for the averaged dynamic model of the robotic fish, are shown in Table I. In particular, the body

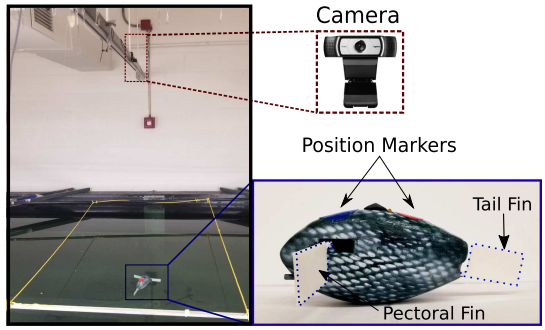

Fig. 3. Experimental setup. During experiments the pectoral-fin actuated robotic fish, depicted on the bottom right, swims within the enclosed area (denoted by the yellow lines) in the tank, and the overhead Logitech camera (depicted on the top right) captures a video of the robot swimming. An image processing algorithm detects the red and blue markers placed on top of the robot to determine its position and heading [16].

TABLE I
Identified Model Parameters for the Robotic Fish [16]

Robot Body		
Parameter	Value	unit
Body Length	0.198	m
Body Height	0.1	m
Body Width (C_P)	0.03	m
Mass (m_b)	0.795	kg
Inertia (J_{bz})	4.26×10^{-4}	kg · m^2
$-m_{ax}$	0.095	kg
$-m_{ay}$	0.1794	kg
$-J_{az}$	2.7×10^{-5}	kg/m^2
Wet surface area (S_A)	0.325	m^2
Drag coef. (C_D)	0.3870	–
Lift coef. (C_L)	0.0808	–
Moment coef. (C_M)	8.5×10^{-3}	kg/m^2

Pectoral Fin		
Parameter	Value	unit
Fin Length (S_p)	0.061	m
Fin Heigth (D_p)	0.041	m
Fin Mass (m_{pf})	0.008	kg
Effective mass (m_p)	0.008	kg
Water density (ρ)	1000	kg/m^3
λ	4.1464	–

drag and lift coefficients $(C_D, C_L, \text{and} C_M)$ and the parameter λ are estimated empirically from data collected using the robotic fish. Specifically, only one fin is activated at a time (e.g., the right fin) such that the robot undergoes a turning motion. After the robot swims for some time and reaches steady-state motion, the actuation of the pectoral fin is stopped, and we use the captured video along with the image processing algorithm to determine the body-fixed velocities for different sets of fin-parameters $(\gamma_{AR}, \gamma_{0R}, T_{pR}, \zeta)$. An extended high-gain observer is used to estimate the body-fixed accelerations, which along with the measured body-fixed velocities and (7), are used to estimate the body drag and lift coefficients parameters via linear regression using the MATLAB command *mldivide*. Similarly, to estimate the fin parameter λ, we collect the the robotic fish's steady-state body-fixed velocities when it undergoes circular motion for a different set of fin parameters $(\gamma_{AR}, \gamma_{0R}, T_{pR}, \zeta)$ and use (7) to employ another linear regression scheme. Finally, to estimate the proper scaling functions, a nonlinear model-predictive control approach is used to find the optimal scaling values for a set of fin-beat patterns, and then a nonlinear regression is used to

determine the scaling functions. We refer the reader to [16] for a more comprehensive description of the parameter estimation procedures.

The robotic fish is run in a 2.3 m by 1.2 m enclosed area within a tank that is equipped with a Logitech C930E overhead camera as seen in Fig. 3. The robotic fish's position and orientation is obtained with two markers, which are attached to the posterior and anterior of the robotic fish body. In particular, the overhead camera captures a video of the robotic fish swimming in the tank, and sends it to a computer via USB, where a Visual C++ with the OpenCV library is used to implement an image processing algorithm, which detects the positions of the two markers. The center position of the robotic fish is then obtained by taking the average, while the heading angle of the robot is estimated using the positions of the two markers. Finally, a high gain observer is used to estimate the linear and angular velocities of the robot based on the measured position and heading angle. Using the measured and estimated states, the control input is then computed by the computer, and the pectoral fin-beat parameters are send wireless via XBee to the robotic fish's microcontroller for implementation.

B. Trajectory Tracking Results

Experiments are carried out to compare the performance of the proposed backstepping-based controller with that of a PID controller. To design the PID controller, we consider a vector $\vec{r}_e$ from the center of the robot (X, Y) to the point $(X_r(t), Y_r(t))$ on the trajectory. We let r_e be the distance between $(X_r(t), Y_r(t))$ and (X, Y), and ϕ_e be the orientation error, defined as the angle between the robotic fish heading direction ψ and the line connecting the body center (X, Y) to the point on the trajectory $(X_r(t), Y_r(t))$. Ensuring that the pair (r_e, ϕ_e) converges to zero implies that the trajectory tracking goal is achieved. With (r_e, ϕ_e), we can then design two PID controllers to find γ_{AR} and γ_{AL}. In particular, the error r_e is used to design the first PID controller, which determines the quantity $u_{p1} = \gamma_{AR} + \gamma_{AL}$ and the error ϕ_e is used to design the second PID, which determines $u_{p2} = \gamma_{AR} - \gamma_{AL}$. Using u_{p1}, u_{p2} one can then solve for γ_{AR} and γ_{AL}. To determine ζ_f, the inner product between $\vec{r}_e$ and the body-fixed unit vector $\hat{x}$ is considered. In particular, when the robot is ahead of the trajectory and the inner product is negative, $\zeta_f = \zeta_{f_{\min}}$, so that the robot can swim backward toward the trajectory. Similarly, when the robot is behind the trajectory and the inner product is positive, $\zeta_f = \zeta_{f_{\max}}$ such that the robot can swim forward. Finally, to account for the actuator constraints, the original calculated values for the pectoral fin-beat parameters are saturated to obtain the realizable values and thus the viable inputs. The following parameters are used for the proposed controller in the experiments:

$$K_{\bar{X}e} = 0.5\, K_{\bar{Y}e} = 0.5\, K_{\bar{\psi}e} = 0.6\, K_1 = 0.55$$
$$K_2 = 0.58\, K_3 = 0.6\, \zeta_1 = 0.05\, \zeta_2 = 0.05$$
$$\zeta_3 = 0.1\, \zeta_4 = 0.2\, \zeta_5 = 0.4\, \zeta_6 = 0.4$$
$$\gamma_{A_{\min}} = 0^\circ \gamma_{A_{\max}} = 40^\circ\, T_{pR} = 1 \text{ s}\, T_{pL} = 1 \text{ s}$$
$$\zeta_{f_{\min}} = \frac{1}{3.5}\zeta_{f_{\max}} = 3.5 t_s = 1 \text{ s} Q_x = 700$$
$$Q_y = 690 Q_z = 640000$$

where $K_{\bar{X}e}, K_{\bar{Y}e}, K_{\bar{\psi}e}, K_1, K_2, K_3, \zeta_1, \zeta_2, \zeta_3, \zeta_4, \zeta_5, \zeta_6$ are tuning parameters for the backstepping controller and auxiliary system. The backstepping controller and auxiliary system parameters were tuned such that the controller was able to stabilize the error system at the origin. We found that, by varying $K_{\bar{X}e}, K_{\bar{Y}e}$, and $K_{\bar{\psi}e}$, we could control the convergence rate of X_e, Y_e, and ψ_e, respectively. Furthermore, varying $\zeta_1 - \zeta_6$ controlled the convergence rate of $\lambda_1 - \lambda_6$, which are the errors that arise as a consequence of the effect of the input constraints. The weights for the forces Q_x, Q_y and the moment Q_w are disproportionate to account for the difference in scale between the body-fixed forces and the moment. t_s is the control sampling interval, i.e., the amount of time between updates to the control inputs. In this article, we choose t_s= 1 s given that the pectoral fin-beat period is 1 s. The optimization problem (39) takes on average 0.35 s to solve, and is thus well within the sampling period. Finally, the PID controller parameters are chosen as

$$K_{P1} = 3.06\ K_{P2} = 3.06\ K_{I1} = 0.02$$
$$K_{I2} = 0.15\ K_{D1} = 0.15\ K_{D2} = 0.1$$

where $K_{P1}, K_{P2}, K_{I1}, K_{I2}, K_{D1}$, and K_{D2} were tuned experimentally using the Ziegler–Nichols closed-loop method [28].

The following reference trajectory (X_r, Y_r, ψ_r) for the robotic fish position and orientation is used in experiments

$$\begin{cases} \dot{X}_r = u_r \cos\psi_r, \quad \dot{Y}_r = u_r \sin\psi_r \\ \dot{\psi}_r = \omega_r, \quad \psi_r(0) = \pi \quad \text{with} \\ u_r = -0.005 \text{ m/s}, \quad \omega_r = 0 \text{ rad/s}, \quad t < 30 \\ u_r = -0.005 \text{ m/s}, \quad \omega_r = 0.01 \text{ rad/s}, \quad 30 \le t < 35 \\ u_r = -0.005 \text{ m/s}, \quad \omega_r = 0.02 \text{ rad/s}, \quad 35 \le t < 150 \\ u_r = 0.007 \text{ m/s}, \quad \omega_r = 0 \text{ rad/s}, \quad 150 \le t < 180 \\ u_r = 0.004 \text{ m/s}, \quad \omega_r = -0.02 \text{ rad/s}, \quad 180 \le t \end{cases}$$

where $\dot{X}_r$ and $\dot{Y}_r$ are the velocity of the reference trajectory in the inertial frame, and u_r, ω_r represent the body-fixed velocities used to generate the reference trajectory that satisfies the kinematic constraints of the robot. Note that with the above choice of u_r and ω_r with step changes, the robot is tasked to perform different, challenging maneuvers with abrupt changes in between. For example, the robot is required to swim backwards in a straight line during $0 \le t < 30$, followed by swimming backward in a circular motion during $30 \le t < 150$. Five different trials with similar initial conditions are performed for both the proposed backstepping-based controller and the PID controller. In Fig. 4, the reference and the achieved trajectories of the robotic fish for one of the experimental trials are compared. The reference trajectory is given by the green solid line, and the blue and red diamond depicts the starting position of the robot while the green circle depicts the start point of the reference trajectory.

In addition, Fig. 5 depicts the averaged position tracking error trajectory over time for both control schemes. This error is obtained by averaging the tracking errors across all five trials. In particular, the solid blue line with diamond markers represents

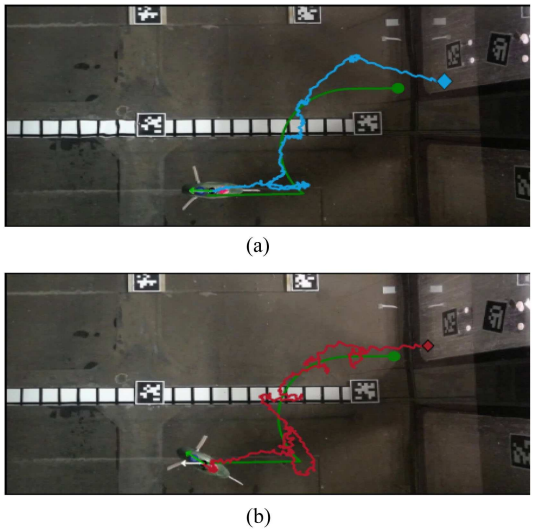

Fig. 4. Experiments: A snapshot of an experimental run for variable trajectory-tracking using (a) the proposed backstepping-based control and (b) the PID control, respectively. The white arrow and the green represent the desired and actual robot orientations, respectively. A video of these experimental results is shown at https://youtu.be/iAH3D5rEZ7M.

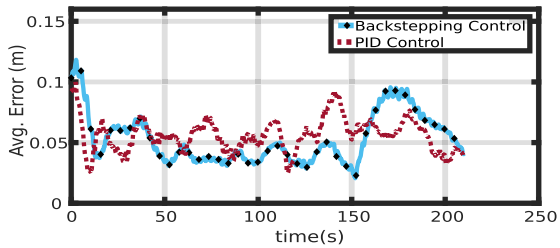

Fig. 5. Experiments: averaged position error for backstepping-based control and PID control.

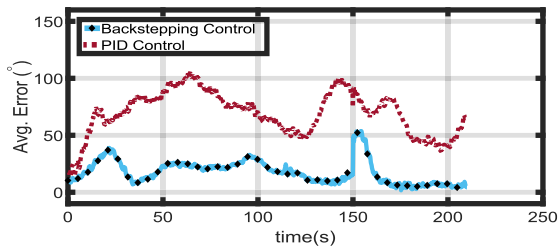

Fig. 6. Experiments: averaged angle error for backstepping-based control and PID control.

the averaged tracking error obtained for backstepping-based control, while the dotted red line represents the averaged error obtained for PID control. Similarly, Fig. 6 depicts the averaged orientation tracking error over time for both control schemes. Fig. 7 depicts the overall average position and angle error scores together with its standard deviation, where each of these errors is obtained by averaging the corresponding tracking error over time. Finally, Fig. 8 depicts the averaged control effort for both the backstepping and PID controllers. The control effort is obtained by summing the integrals of the right fin and the left

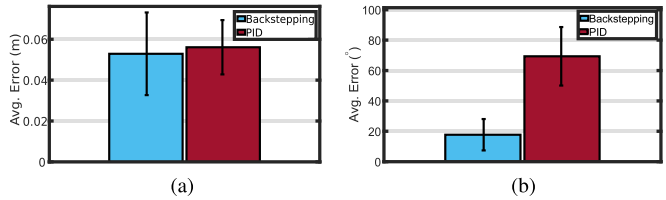

Fig. 7. Experiments: (a) averaged position error scores and (b) averaged angle error scores for backstepping-based control and PID control. The two subplots compare the performance for the overall position and angle error scores in tracking the variable reference trajectory. Each error score is obtained by averaging the corresponding position or orientation error over time. The error bars indicate the standard deviation of the error score (over time).

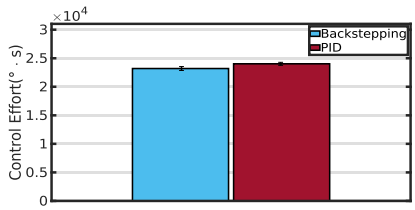

Fig. 8. Experiments: Averaged control effort for backstepping-based control and PID control.

fin's amplitudes over time, and then taking the average over the five trials.

From Fig. 5, it can be noted that the proposed backstepping scheme achieves better performance, on average, to the PID controller in terms of the position tracking error. This is more evident from Fig. 7(a), as the proposed approach obtains a smaller overall error score. The difference in the performance between the proposed approach and the PID is highlighted in the tracking of the desired orientation. In particular, from Fig. 6, we can see that the proposed approach was able to track the desired orientation with a relatively small error when compared to PID and achieves a smaller steady-state error (about 4.5° on average). In addition, from Fig. 7(b) we can see that the proposed approach significantly outperforms PID, overall, in terms of the orientation error. Note that the proposed approach allowed the robot to respond to the sudden changes in the desired heading (particularly at $t \geq 150$), and thus decrease the orientation error relatively quickly. Finally, from Fig. 8 we see that on average the proposed control method spent less effort than the PID controller, which shows an additional benefit of the proposed approach.

We note that the PID controller and the proposed controller have two different methods of constructing the orientation error, which likely have contributed to the performance difference in orientation tracking. Unfortunately, given the available system inputs, it is challenging to design a PID controller that can simultaneously address position tracking and orientation tracking explicitly, which speaks for the limitation of the PID approach in dealing with nonlinear multi-input-multi-output systems. In contrast, the proposed control approach presents a systematic design procedure and exploits the system dynamics to balance position tracking and orientation tracking.

V. Conclusion

In this article, we proposed a backstepping-based trajectory tracking controller for a pectoral fin-actuated robotic fish. In particular, we proposed a dual-loop scheme that uses an outer loop backstepping-based controller designed based on an averaged model and an inner loop multivariable minimization solver to determine the optimal fin-beat parameters. The proposed scheme was implemented on a pectoral fin-actuated robotic fish, and real-time experimental results demonstrated the effectiveness of the proposed scheme and showed its value over standard PID control. In particular, from the position and orientation error scores, the proposed backstepping-based approach has better performance than PID in terms of tracking the position, but it greatly outperforms PID in tracking the desired orientation. The proposed controller also shows a distinct advantage in adapting to sudden changes in the reference trajectory. Finally, the proposed method was shown to use less control effort than the PID controller. Therefore, by exploiting the knowledge of the average model, the proposed scheme exhibits multiple advantages in performance over the PID controller at the moderate computational expense.

For future work, the controller will be evaluated in an environmental sensing application, where there will be an upper level path planning scheme integrated with the backstepping-based trajectory-tracking scheme. In addition, since the original dynamic model captures transient behavior while the averaged dynamic model captures the steady state behavior, the proposed controller will be utilized to develop a framework that allows the coordination of the proposed approach and rapid maneuvering controller design using the original dynamics (as done in [21]). Finally, since the tail fin tends to be most beneficial at higher speeds, while pectoral fins tend to be more effective for maneuvering, we will explore the coordination control of the two forms of locomotion.

References

[1] X. Tan, "Autonomous robotic fish as mobile sensor platforms: Challenges and potential solutions," *Mar. Technol. Soc. J.*, vol. 45, no. 4, pp. 31–40, 2011.

[2] F. Zhang, O. Ennasr, E. Litchman, and X. Tan, "Autonomous sampling of water columns using gliding robotic fish: Algorithms and harmful-algae-sampling experiments," *IEEE Syst. J.*, vol. 10, no. 3, pp. 1271–1281, Sep. 2016.

[3] S. Marras and M. Porfiri, "Fish and robots swimming together: Attraction towards the robot demands biomimetic locomotion," *J. Roy. Soc. Interface*, vol. 9, no. 73, pp. 1856–1868, 2012.

[4] M. Sfakiotakis, D. M. Lane, and J. B. C. Davies, "Review of fish swimming modes for aquatic locomotion," *IEEE J. Ocean. Eng.*, vol. 24, no. 2, pp. 237–252, Apr. 1999.

[5] S. B. Behbahani, "Role of flexibility in robotic fish," Ph.D. dissertation, Dept Elect. Comput. Eng., Michigan State Univ., East Lansing, MI, USA, 2016.

[6] S. Vogel, *Life in Moving Fluids: The Physical Biology of Flow*. Princeton, NJ, USA: Princeton Univ. Press, 1996.

[7] M. Wang, J. Yu, M. Tan, and J. Zhang, "Multimodal swimming control of a robotic fish with pectoral fins using a CPG network," *Chin. Sci. Bull.*, vol. 57, no. 10, pp. 1209–1216, 2012.

[8] K. A. Morgansen, T. M. La Fond, and J. X. Zhang, "Agile maneuvering for fin-actuated underwater vehicles," in *Proc. 2nd Int. Symp. Commun., Control Signal Process.*, 2006.

[9] M. Wang, J. Yu, and M. Tan, "Modeling neural control of robotic fish with pectoral fins using a CPG-based network," in *Proc. 48th IEEE Conf. Decis. Control 28th Chin. Control Conf.*, 2009, pp. 6502–6507.

[10] M. Wang, J. Yu, M. Tan, and J. Zhang, "Design and implementation of a novel CPG-based locomotion controller for robotic dolphin," in *Proc. 8th World Congr. Intell. Control Autom.*, 2010, pp. 1611–1616.

[11] J. Yu, K. Wang, M. Tan, and J. Zhang, "Design and control of an embedded vision guided robotic fish with multiple control surfaces," *Sci. World J.*, vol. 2014, 2014, Art. no. 631296.

[12] S. Zhang, Y. Qian, P. Liao, F. Qin, and J. Yang, "Design and control of an agile robotic fish with integrative biomimetic mechanisms," *IEEE/ASME Trans. Mechatronics*, vol. 21, no. 4, pp. 1846–1857, Aug. 2016.

[13] M. Wang, J. Yu, and M. Tan, "CPG-based sensory feedback control for bio-inspired multimodal swimming," *Int. J. Adv. Robotic Syst.*, vol. 11, no. 10, pp. 170–180, 2014.

[14] N. Kato, "Control performance in the horizontal plane of a fish robot with mechanical pectoral fins," *IEEE J. Ocean. Eng.*, vol. 25, no. 1, pp. 121–129, Jan. 2000.

[15] K. A. Morgansen, B. I. Triplett, and D. J. Klein, "Geometric methods for modeling and control of free-swimming fin-actuated underwater vehicles," *IEEE Trans. Robot.*, vol. 23, no. 6, pp. 1184–1199, Dec. 2007.

[16] M. L. Castaño and X. Tan, "Averaged modeling of pectoral fin-actuated robotic fish," *IFAC-PapersOnLine*, vol. 54, no. 20, pp. 114–121, 2021.

[17] R. Prakash, L. Behera, S. Mohan, and S. Jagannathan, "Dual-loop optimal control of a robot manipulator and its application in warehouse automation," *IEEE Trans. Automat. Sci. Eng.*, vol. 19, no. 1, pp. 262–279, Jan. 2022.

[18] C. Yang, Y. Shi, L. Li, and X. Wang, "Efficient mode transition control for parallel hybrid electric vehicle with adaptive dual-loop control framework," *IEEE Trans. Veh. Technol.*, vol. 69, no. 2, pp. 1519–1532, Feb. 2020.

[19] R. Zhu, Z. Chen, Y. Tang, F. Deng, and X. Wu, "Dual-loop control strategy for DFIG-based wind turbines under grid voltage disturbances," *IEEE Trans. Power Electron.*, vol. 31, no. 3, pp. 2239–2253, Mar. 2016.

[20] M. L. Castaño and X. Tan, "Backstepping control-based trajectory tracking for tail-actuated robotic fish," in *Proc. IEEE/ASME Int. Conf. Adv. Intell. Mechatronics*, 2019, pp. 839–844.

[21] M. L. Castaño and X. Tan, "Rapid maneuvering control of pectoral fin-actuated robotic fish," in *Proc. IEEE/ASME Int. Conf. Adv. Intell. Mechatronics*, 2021, pp. 705–712.

[22] M. L. Castaño and X. Tan, "Model predictive control-based path-following for tail-actuated robotic fish," *J. Dyn. Syst., Meas., Control*, vol. 141, no. 7, 2019, Art. no. 071012.

[23] J. Wang and X. Tan, "Averaging tail-actuated robotic fish dynamics through force and moment scaling," *IEEE Trans. Robot.*, vol. 31, no. 4, pp. 906–917, Aug. 2015.

[24] M. Aureli, V. Kopman, and M. Porfiri, "Free-locomotion of underwater vehicles actuated by ionic polymer metal composites," *IEEE/ASME Trans. Mechatronics*, vol. 15, no. 4, pp. 603–614, Aug. 2010.

[25] S. B. Behbahani and X. Tan, "Role of pectoral fin flexibility in robotic fish performance," *J. Nonlinear Sci.*, vol. 27, no. 4, pp. 1155–1181, 2017.

[26] J. Farrell, M. Polycarpou, and M. Sharma, "Adaptive backstepping with magnitude, rate, and bandwidth constraints: Aircraft longitude control," in *Proc. Amer. Control Conf.*, 2003, pp. 3898–3904.

[27] K. Deb, *Multi-Objective Optimization Using Evolutionary Algorithms*, Hoboken, NJ, USA: Wiley, 2001.

[28] F. Haugen, *PID Control*. Trondheim, Norway: Tapir Academic Press, 2004, pp. 94–98.